

## **Thermal performance enhancement of flat plate solar air heater using transverse U-shaped turbulator - A numerical study**

**M. S. Manjunath<sup>1</sup>, R. Venkatesh<sup>1</sup> and Madhwesh N<sup>2\*</sup>**

<sup>1</sup>School of Engineering and IT, Manipal Academy of Higher Education, Dubai Campus, DIAC-G-008, International Academic City, P.O. Box 345050, Dubai, UAE

<sup>2</sup>Department of Mechanical and Manufacturing Engineering, Manipal Institute of Technology, Manipal Academy of Higher Education, Manipal, Karnataka, India, 576104.

\*Email: [madhwesh.n@gmail.com](mailto:madhwesh.n@gmail.com)

Phone: +91 98809 40050

### **ABSTRACT**

The aim of this study is to determine the effect of U-shaped rib turbulator on the flow and heat transfer characteristics of flat plate solar air heater using two-dimensional Computational Fluid Dynamics (CFD) analysis. The analysis is carried out using the CFD software tool ANSYS Fluent 15.0 for the flow Reynolds number ranging from 9000 to 21,000. The relative pitch ( $P/e$ ) of the U-shaped rib is varied as 5, 10, 25 and 40 for a fixed relative rib height of 0.0421. It is shown that the U-shaped rib augments the Nusselt number by about 1.76 times while the friction factor increased by about 1.95 times with reference to smooth duct for a relative pitch of 10 and 5 respectively. The maximum thermal enhancement factor is obtained as 1.5 for the configuration of  $P/e=25$ . A comparative analysis of U-shaped rib with circular rib reveals that the U-shaped rib turbulator is found to be more effective in providing heat transfer enhancement and has about 15% higher thermal enhancement factor as compared to circular turbulator.

**Keywords:** CFD; U-shaped turbulator; solar air heater; rib turbulator; enhanced heat transfer.

### **INTRODUCTION**

The ever increasing energy demand for domestic as well as industrial applications has posed a big challenge in handling the global climate change, ozone deterioration and global warming issues. Increased urbanization and changing lifestyle has greatly increased the energy supply requirements of domestic as well as industrial buildings. Hence, in order to reduce the energy supply load based on fossil fuels, it is relevant and compelling to think of alternative sources of energy supply such as solar energy to supply part of the building energy needs. Much of the building energy needs come from the HVAC systems for space heating and cooling applications. The space heating needs could be partly met by a solar air heater. Besides space heating applications, solar air heaters are also widely used in food industries for drying of spices, tea, coffee, fish, paddy etc., and drying of timber. In fact, a combined solar and biomass air dryer has been found to be more convenient [1]. Flat plate solar air

heaters are simple in design construction and operation and have low maintenance cost. Its biggest advantage is the ability to absorb both diffuse and direct solar radiation incident on the absorber plate. However, they have higher thermal losses and the working fluid which is air, further adds to the performance issues as it is characterized by poor heat transfer capabilities. As a result, flat plate solar air heaters typically operate at lower levels of thermal efficiency. In this regard, there has been lot of efforts in the past to provide design improvements so as to achieve higher thermal efficiency. Heat transfer enhancement through augmented turbulence levels in the fluid is a well-known concept and is widely used in solar air heater applications. Enhancement of fluid turbulence using turbulators over the absorber plate has been the most commonly used technique. Turbulators generate local disturbances in the air flow by creating flow separation around them thereby breaking the laminar sub-layer of the turbulent flow leading to increased heat energy transfer from the heated plate thereby enhancing the thermal efficiency of the system. However, the modifications done on the absorber plate to achieve higher fluid turbulence also increase the flow resistance resulting in higher pressure drop penalty. Therefore, the focus of most of the studies in the past has been to develop such turbulence enhancement elements which would provide higher heat transfer rates with least flow resistance. This is possible by determining the optimum operating parameters such as the flow Reynolds number and optimum design parameters such as the turbulator geometry, pitch distance, inclination of turbulator to the flow, height of turbulator and arrangement pattern of turbulators. In this regard, the focus of most of the earlier studies has been on the fundamental aspect of varying the turbulator cross-sectional geometry such as the square sectioned rib [2, 3], square sectioned wave profiled rib [4], chamfered square ribs [5], transverse circular ribs [6, 7], semi-circular ribs [8], isosceles triangular rib [9], right angled triangular ribs [10], equilateral triangular ribs [11], wedge shaped ribs [12], hyperbolic ribs [13], reverse L-shaped ribs [14], rectangular sectioned tapered ribs [15], rib-grooved artificial roughness [16] and forward facing chamfered rectangular sectioned ribs [17]. Each geometry has been shown to produce different levels of overall thermal performance. Use of S-baffles [18], conical pin arrangement [19] have also been shown to provide considerable heat transfer improvement. The chamfered square rib turbulators have been shown to have a relatively higher friction factor enhancement of about 4.248 times the plain duct with a maximum thermal enhancement factor of about 2.047 while the transverse semi-circular rib turbulators have been reported to have a relatively lower rise in friction factor of about 1.92 times the plain duct with a maximum thermal enhancement factor of about 1.71. This is due to the varying levels of flow disturbance generated by different geometries of the rib. The flow structure on both the sides of rib has significant influence on pressure drop as well as heat transfer. The wedge-shaped ribs have been shown to significantly vary the flow structure depending on the angle of wedge and have a relatively smaller recirculation zones on the downstream side. Use of hyperbolic ribs significantly reduce the entrapped eddies on both sides of the rib thereby providing improved heat transfer and reduced friction factor penalty. In another area of research, Kamali and Binesh [20] carried out numerical investigations to evaluate the influence of square, triangle and trapezoidal cross-section ribs on the changes in flow behavior in the intermediate region of the ribs. They have reported that the rib geometry has a significant effect on the flow structure and hence the heat transfer. A more detailed numerical analysis to evaluate the influence of rib shape on the flow structure has been carried out by Zheng et al.[21] who made modifications to square ribs to obtain different cross-sectional shapes of ribs such as

chamfered ribs, concave ribs and convex ribs. They found that the rib cross-sectional geometry significantly influences the flow structure in the downstream region and the introduction of streamlined edges reduced the entrapped smaller vortex zones thereby enhancing the heat energy interaction. Therefore, it is an established fact that the turbulator cross-sectional geometry has strong influence on the flow behavior as a result of which different geometries create different levels of thermal performance enhancement. This served as motivation to carry out the current study to evaluate the effect of a novel U-shaped geometry on the influence of overall thermal performance of flat plate solar air heater system. It is observed that there has not been any reported work on the use of U-shaped rib turbulator and most of the previous works focused on the standard turbulator geometries. Thus, the objective of this work is to conduct a two-dimensional CFD simulation study to evaluate the efficacy of novel transverse U-shaped turbulator with respect to smooth duct for different flow Reynolds number conditions. The effect of number of turbulators on the overall thermal performance will be brought out for a fixed relative rib height of 0.0421.

## **PERFORMANCE PARAMETERS USED IN THE ANALYSIS**

### **Nusselt Number**

The average value of Nusselt number for roughened duct is calculated using the equation given by,

$$Nu_r = \frac{hD}{k} \quad (1)$$

Where, the area weighted average value of convective heat transfer coefficient ‘ $h$ ’ (W/m<sup>2</sup>K) is obtained from ANSYS Fluent software for different flow Reynolds number conditions.

### **Friction Factor**

The friction factor for roughened duct is calculated using Equation (2) based on the pressure drop value obtained from ANSYS Fluent software across the duct of length 0.64 m.

$$f_r = \frac{\Delta p D}{2\rho LV^2} \quad (2)$$

### **Thermal Enhancement Factor**

The effective thermal performance is evaluated using thermal enhancement factor given by,

$$TEF = \frac{\left( \frac{Nu}{Nu_r} \right)}{\left( \frac{f}{f_r} \right)^{1/3}} \quad (3)$$

## CFD ANALYSIS

### Calculation Domain of Air Duct Fixed with U-shaped Turbulator

Figure 1 shows the geometric details of calculation domain of air duct fixed with transverse U-shaped turbulator used for the CFD analysis and the details of dimensions of air duct are listed in Table 2. The U-shaped turbulators are placed transversely on the absorber plate and the design parameters of turbulator such as relative pitch which decides the number of turbulators and relative height which decides the extent of protrusion of turbulator into the air duct are listed in Table 3. The rib height is so chosen so as to have a non-dimensional rib height as 0.0421 which is an optimum height for enhanced heat transfer [2-3].

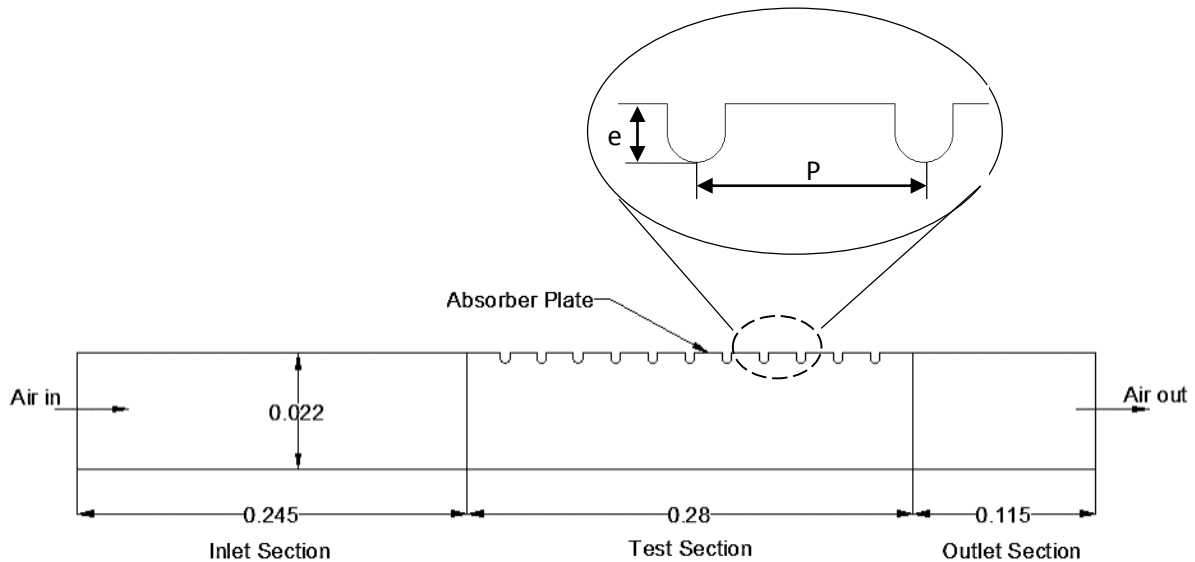


Figure 1. Calculation domain of air duct fixed with U-shaped turbulator (All dimensions in m).

Table 2. Various geometric parameters of air duct

Parameter	Value (m)
Length of inlet section	0.245
Length of test section	0.280
Length of exit section	0.115
Height of duct, 'H'	0.022
Width of duct, 'W'	0.150
Hydraulic diameter of duct, 'D'	0.038

Table 3. Design parameters of turbulators used in the analysis

Relative pitch, P/e	Pitch, P (m)	Height of rib, e (m)	Relative rib height, e/D
5	0.008		
10	0.016		
25	0.040	0.0016	0.042
40	0.064		

### Governing Equations

The mean flow equations that govern the two-dimensional turbulent flow and heat transfer are as follows:

Continuity equation:

$$\frac{\partial}{\partial x_i}(\rho u_i) = 0 \quad (4)$$

Momentum equation:

$$\frac{\partial}{\partial x_i}(\rho u_i u_j) = -\frac{\partial p}{\partial x_i} + \frac{\partial}{\partial x_j} \left[ \mu \left( \frac{\partial u_i}{\partial x_j} + \frac{\partial u_j}{\partial x_i} \right) \right] + \frac{\partial}{\partial x_j} (\overline{-\rho u_i u_j}) \quad (5)$$

Energy equation:

$$\frac{\partial}{\partial x_i}(\rho u_i T) = \frac{\partial}{\partial x_j} \left[ (\Gamma + \Gamma_t) \frac{\partial T}{\partial x_j} \right] \quad (6)$$

The RNG k-ε turbulence model is given by,

$$\frac{\partial}{\partial x_i}(\rho k u_i) = \frac{\partial}{\partial x_j} \left( \alpha_k \mu_{eff} \frac{\partial k}{\partial x_j} \right) + G_k - \rho \varepsilon \quad (7)$$

$$\frac{\partial}{\partial x_i}(\rho \varepsilon u_i) = \frac{\partial}{\partial x_j} \left( \alpha_\varepsilon \mu_{eff} \frac{\partial \varepsilon}{\partial x_j} \right) + C_{1\varepsilon} \frac{\varepsilon}{k} G_k - C_{2\varepsilon} \rho \frac{\varepsilon^2}{k} - R_\varepsilon \quad (8)$$

The effective viscosity is given by,

$$\mu_{eff} = \mu + \mu_t \quad (9)$$

The turbulent viscosity is given by,

$$\mu_t = \rho C_\mu \frac{k^2}{\varepsilon} \quad (10)$$

The value of the constants in the above equations are given by,

$C_{1\varepsilon} = 1.42$ ,  $C_{2\varepsilon} = 1.68$  and  $C_\mu = 0.0845$

### Numerical Schemes and Boundary Conditions

The numerical analysis is carried out using the ANSYS Fluent software tool. SIMPLE algorithm is used for effecting the pressure-velocity coupling and second order upwind scheme is used for the discretization of governing equations of flow and energy. The default settings of first order upwind schemes were changed to second order upwind schemes for

increased accuracy. The Renormalization Group (RNG) k-ε turbulence model with enhanced wall treatment is adopted to capture the turbulent flow parameters in the analysis as reported by previous studies [2-5]. Also, a wall y+ value of about 1 is maintained near the solid-fluid interface in order to place the first grid point within the laminar sublayer region of turbulent boundary layer as suggested in ANSYS documentation [22]. The criteria for convergence for flow and energy equations are set as 10<sup>-5</sup> and 10<sup>-8</sup> respectively. The boundary conditions applied to the computational domain are presented in Table 4.

Table 4. Boundary conditions used in the analysis.

Sl. No.	Boundary name	Specified boundary condition	Input values at boundary condition
i.	Duct inlet	Velocity inlet	Uniform velocity ranging between 3.72 m/s and 8.671 m/s with an inlet air temperature of 300 K.
ii.	Duct outlet	Pressure outlet	Atmospheric pressure of 101325 N/m <sup>2</sup> .
iii.	Absorber plate	Constant heat flux	800 W/m <sup>2</sup> .
iv.	Rest of the boundaries of duct	Wall	0 W/m <sup>2</sup> (Insulated wall).

Table 5. Thermo-physical properties of air at 300K.

Sl. No.	Property	Value
i.	Density	1.177 kg/m <sup>3</sup>
ii.	Viscosity	1.8458e-5 Ns/m <sup>2</sup>
iii.	Thermal conductivity	0.02624 W/mK
iv.	Specific heat	1006.43 J/kgK
v.	Prandtl number	0.71

Since, the validation of present CFD results are based on the experimental results of Gupta et al. [23], the same heat flux value of 800 W/m<sup>2</sup> used by them is adopted in the present simulation study. The default heat flux value of 0 W/m<sup>2</sup> in the solver settings is changed to 800 W/m<sup>2</sup> for the absorber plate surface. The default turbulence intensity value of 10% at the core of turbulent flow is replaced by the values obtained through calculation using Equation (11).

$$I = 0.16(\text{Re})^{-1/8} \tag{11}$$

Where, the Reynolds number of the flow is calculated using the equation given by,

$$\text{Re} = \frac{\rho V D}{\mu} \tag{12}$$

The material properties of air used in the analysis are listed in Table 5. The properties such as density, thermal conductivity, specific heat and viscosity are taken at the inlet air temperature conditions of 300 K and are assumed to be constant owing to smaller changes in the air temperature as it flows through the duct.

### Grid Independence Study and Validation of CFD Model

A grid independence test is carried out to arrive at the optimal number of control volumes in the calculation domain followed by the validation of CFD results against the published experimental results of Gupta et al.[23]. For the purpose of validation of proposed CFD model, a two dimensional CFD analysis is carried out for the air duct fitted with circular rib turbulator as shown in Figure 2 and the results are compared against the experimental results of Gupta et al.[23] for the same geometric parameters of circular rib turbulator and operating conditions used in their experiments.

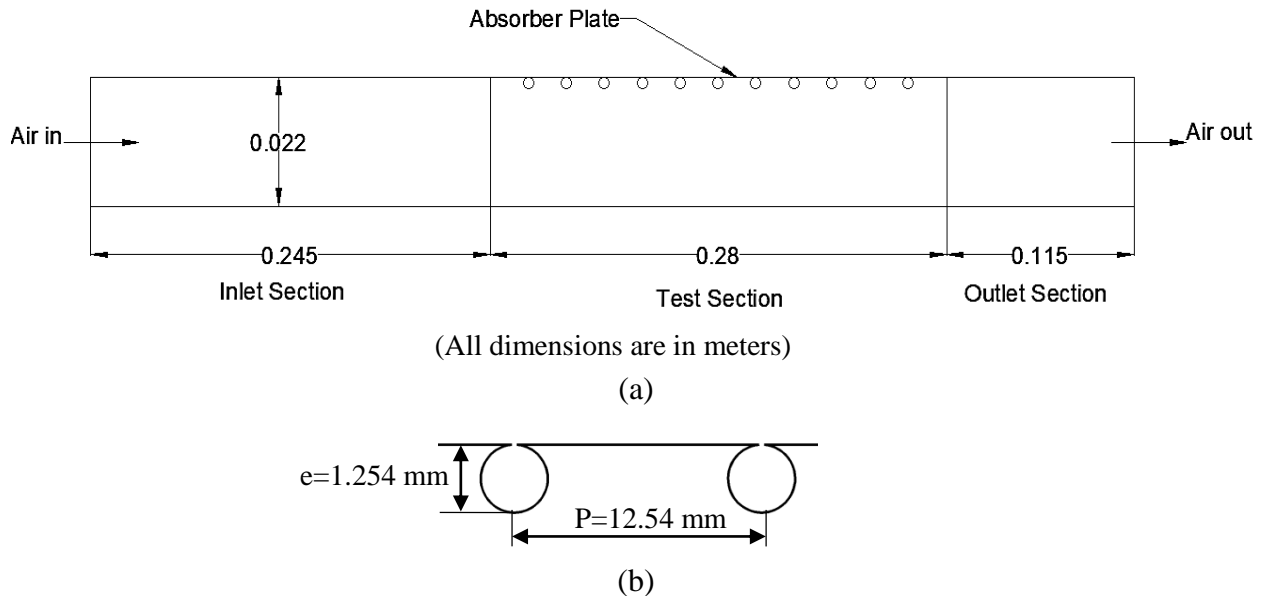


Figure 2. A view of the (a) computational domain of air duct fitted with circular rib turbulator for the validation of proposed CFD methodology and (b) rib parameters used in the experimental study by Gupta et al.[23].

The details of geometric parameters of the computational domain in the presence of circular rib turbulators used by Gupta et al.[23] in their experimental study are given in Table.6. A view of the discretized computational domain with circular rib turbulator is shown in Figure 3. The meshing is carried out using ANSYS meshing tool [22]. Finer control volumes are added in the surrounding region of turbulator and the absorber plate where steep gradients of flow variables are expected. The optimum mesh is arrived at by gradually varying the number of control volumes in the computational domain and the corresponding change in the Nusselt number as well as friction factor are noted for the flow Reynolds number of 18,000 as shown in Table 7. It is seen that the change in Nusselt number is about 0.73% and the variation in friction factor is about 0.44% as the number of control volume increases from 144,557 control volumes to 192,224 control volumes in the computational

domain. Therefore, a minimum of 144,557 control volumes are ensured in all the calculation domain to ensure grid independent solution.

Table 6. Geometric parameters for circular rib turbulator as per Gupta et al.[23]

Sl. No.	Parameter	Value
i.	Width of duct (W)	0.150 m
ii.	Height of duct (H)	0.022 m
iii.	Aspect ratio (W/H)	6.818
iv.	Rib height (e)	1.254e-3 m
v.	Hydraulic diameter of duct (D)	0.038 m
vi.	Relative pitch of rib (P/e)	10

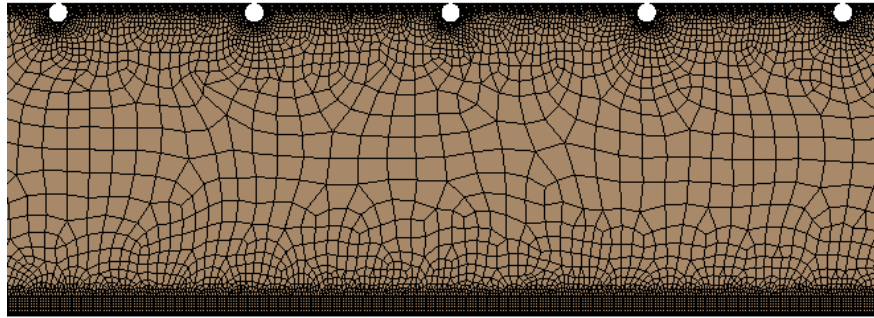


Figure 3. Mesh details of the computational domain with circular rib turbulator.

Table 7. Grid independence test for circular turbulator model.

Number of control volumes	Nusselt number	Variation of Nusselt number (%)	friction factor	Variation of friction factor (%)
52,176	76.31	-	0.01411	-
78,670	75.70	-0.8	0.01438	1.94
99,400	74.31	-1.83	0.01465	1.87
144,557	73.33	-1.32	0.01461	0.25
192,224	72.79	-0.73	0.01455	-0.44
276,306	72.71	-0.12	0.01452	-0.19

Figure 4(a) and Figure 4(b) shows the comparison of CFD results of Nusselt number as well as friction factor against the experimental correlation results reported by Gupta et al. [23] for the flow Reynolds number range of 9000-21,000. The experimental values of Nusselt number and friction factor for circular rib turbulator are reproduced using the correlations reported by them as given by Equation (13) and Equation (14) respectively.

$$Nu_r = 0.000824(e/D_h)^{-0.178} (W/H)^{0.288} (Re)^{1.062} \quad (13a)$$

for  $e^+ \leq 35$

$$Nu_r = 0.00307(e/D_h)^{-0.469} (W/H)^{0.245} (Re)^{0.812} \quad (13b)$$

for  $e^+ \geq 35$

$$f_r = 0.06412(e/D_h)^{0.019} (W/H)^{0.237} (Re)^{-0.185} \quad (14)$$

$$\text{Where, } e^+ = (e/D)Re(f/2)^{0.5} \quad (15)$$

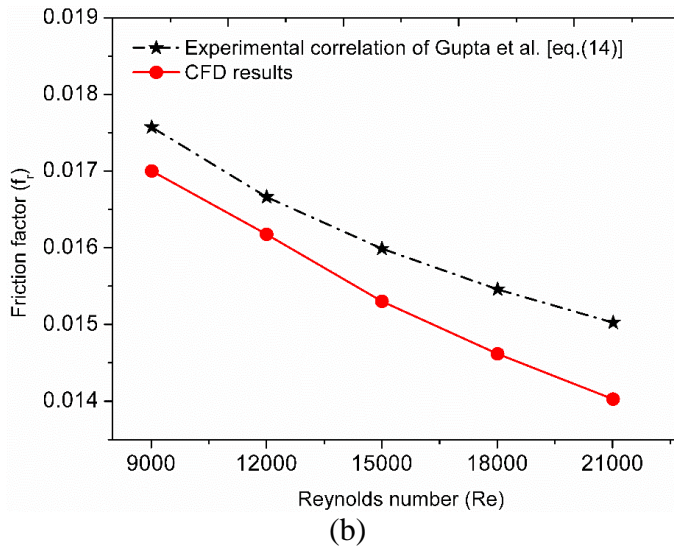
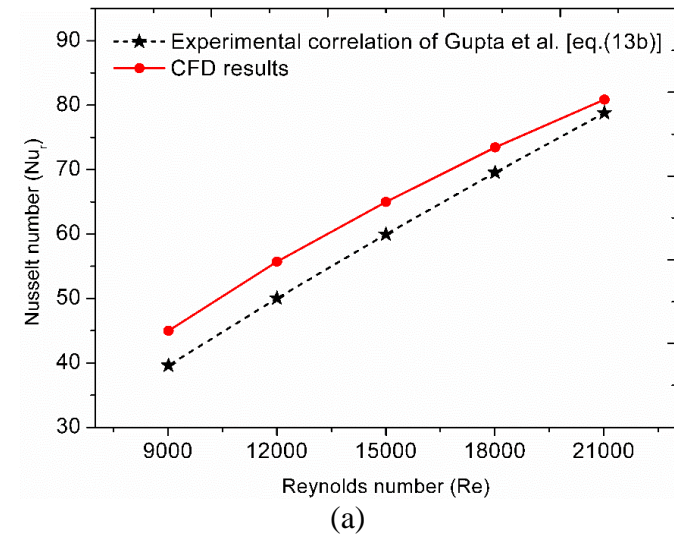


Figure 4. Comparisons of (a) Nusselt number and (b) friction factor results obtained from CFD simulation for circular turbulator against the experimental correlation of Gupta et al [23].

Equation (13b) is used for validation purpose as the  $e^+$  values were found to be between 27 and 60 for the flow rates and relative rib height used in the analysis. The CFD

simulation results of Nusselt number as well as friction factor are found to match closely with the experimental correlation results given by Equation (13b) and Equation (14) and the average deviation for Nusselt number is about 8.31% while it is about 4.51% for friction factor. Hence, the proposed CFD model with the specified boundary conditions, number of control volumes and numerical schemes is deemed good enough to produce results that are in close agreement with experimental ones. The CFD results for friction factor are found to be lower than the experimental results owing to greater resistance to air flow from the walls of the actual air duct as compared to the smooth duct assumption in CFD simulation study. The CFD Nusselt number is relatively higher than experimental owing to heat losses in the air duct in real conditions as compared to adiabatic wall conditions assumed in the simulation study. This CFD methodology is extended with greater confidence in the foregoing analysis wherein the circular turbulator is replaced by the U-shaped turbulator in the computational domain. The mesh of the computational domain with U-shaped rib turbulator is shown in Figure 5.

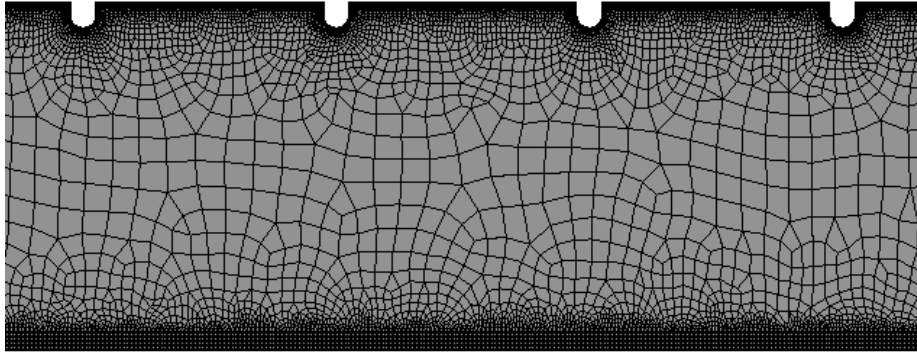


Figure 5. Mesh details of the computational domain with U-shaped turbulator.

## RESULTS AND DISCUSSIONS

### Heat Transfer Characteristics

Figure 6 shows the comparison of Nusselt number for the configuration of U-shaped turbulator for varying relative pitch values of 5, 10, 25 and 40 for the Reynolds number ranging between 9000 and 21,000. The results are compared against the Nusselt number results of smooth duct which are obtained using the well-known Dittus-Boelter equation given by,

$$Nu_{smooth} = 0.023 Re^{0.8} Pr^{0.4} \quad (16)$$

The results show that the Nusselt number increases considerably in the presence of U-shaped turbulator for all the pitch values considered in the analysis with reference to the smooth duct. This is because the presence of U-shaped turbulator disturbs the flow by causing flow separation at the tip of turbulator thereby generating turbulent recirculation zone on the immediate downstream region of the rib as shown in Figure 7 which depicts the pathlines of air flow across the U-shaped rib for the flow Reynolds number of 15,000. As a result, the laminar sub-layer of the turbulent boundary layer which is the main cause for poor heat

transfer between the absorber plate and air would be disturbed. The separated flow subsequently reattaches with the absorber plate in the region between the ribs thereby bringing the relatively colder air from the core of duct in contact with the absorber plate as shown in Figure 7 which leads to enhanced heat transfer. A small recirculation region is also formed at the immediate upstream region of the rib due to backward deflection of the incoming flow. The recirculation zones on either side of the rib create intense mixing within the air flow thereby enhancing the turbulence levels and hence the heat energy exchange. This flow behavior is observed at all the turbulators on the absorber plate which leads to local enhancement of heat transfer. Thus, it is seen that the presence of flow separation, turbulent recirculation zones and flow reattachment provides enhanced heat transfer in the presence of U-shaped rib turbulator.

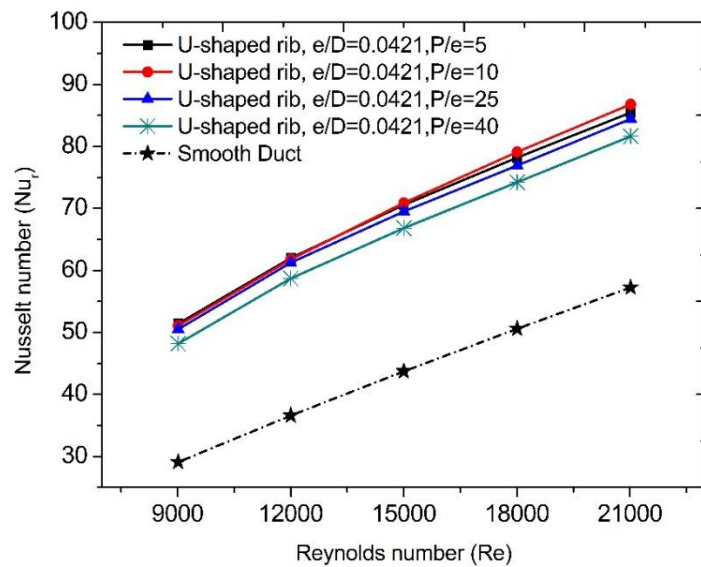


Figure 6. Comparison of Nusselt number for U-shaped turbulator having  $e/D=0.0421$  and  $P/e= 5, 10, 25$  and  $40$ .

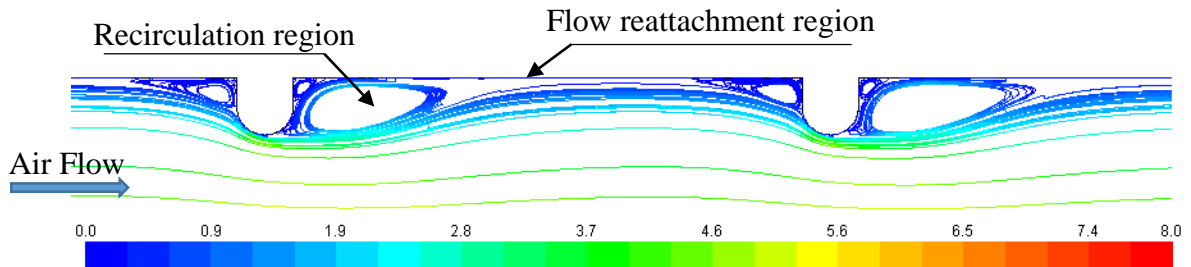


Figure 7. Pathlines (colored by velocity) of air flow across the U-shaped rib turbulator for  $P/e=10$  and  $e/D=0.0421$  at  $Re=15,000$ .

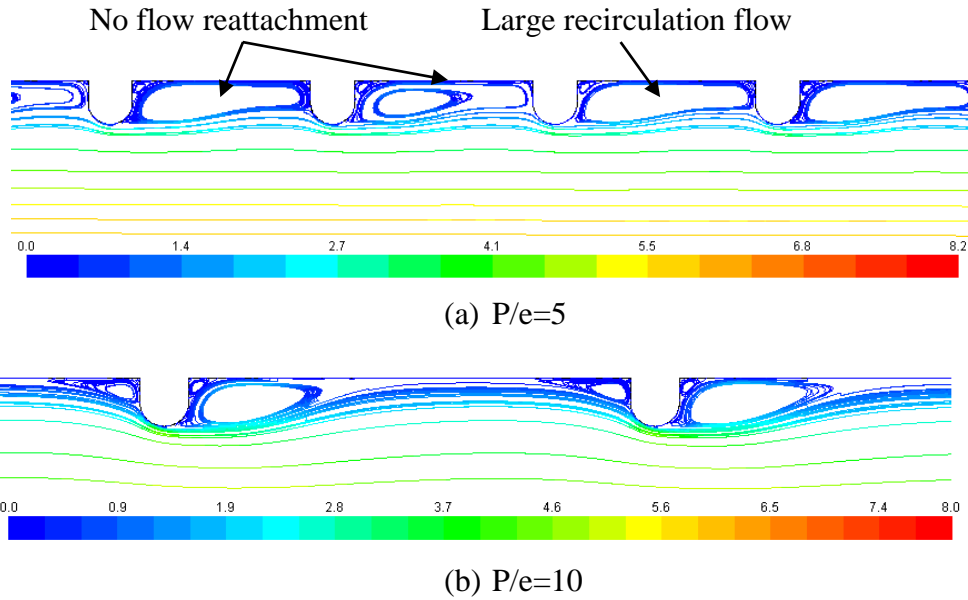


Figure 8. Pathlines of air flow across the rib for U-shaped rib turbulator for (a)  $P/e=5$  and (b)  $P/e=10$  at  $Re=15,000$ .

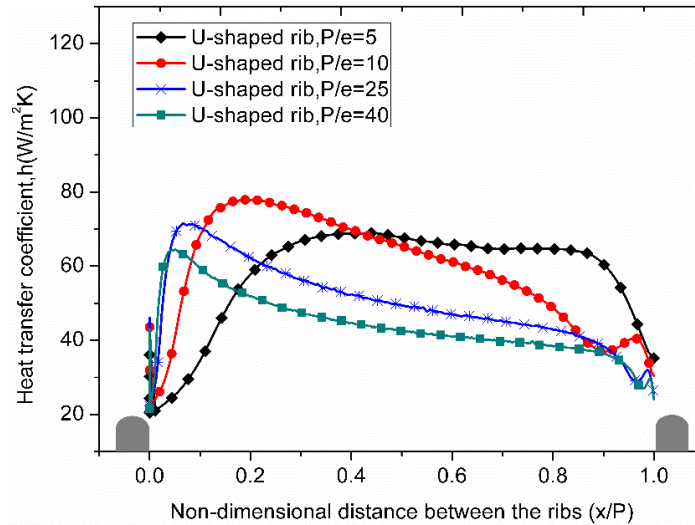


Figure 9. Comparison of heat transfer coefficient for U-shaped rib turbulator for  $P/e=5, 10, 25$  and  $40$  at  $Re=15,000$ .

From Figure 6, it is interesting to see that the Nusselt number increases as the relative pitch increases from 5 to 10 and then decreases with further increase of relative pitch from 25 to 40. This is due to the fact that, for a relative pitch of 5, the turbulators are placed too close to each other and the separated flow is never reattached with the absorber plate in the region between the ribs as shown in Figure 8. As a result, a larger recirculation zone covering the entire inter-rib region is formed and the separated flow is forever detached from the absorber plate leading to limited heat energy exchange from the absorber surface as revealed by the

pathline plot in Figure 8(a). However, as the relative pitch increases to 10, the rib spacing is sufficient enough to allow for flow reattachment on the immediate upstream side of the subsequent rib as displayed in Figure 8(b). As the relative pitch increases further from 25 to 40, the number of turbulators decreases thereby reducing the number of instances of flow separation, recirculation region and reattachment point. In addition, owing to larger pitch distances between successive ribs at larger relative pitch values, the distance between the reattachment point and the successive rib also increases. As a result, the length of laminar sub-layer which reappears after flow reattachment in the inter-rib region also increases before it is disturbed by the subsequent rib. The reappearance of laminar sub-layer hinders the heat energy exchange between the absorber plate and the flowing air stream. This can be further verified by comparing the variation of heat transfer coefficient in the region between the ribs as depicted in Figure 9. It can be seen that the heat transfer coefficient is higher for the relative pitch value of 10. However, as the relative pitch increases beyond 10, the length of flow after reattachment increases leading to an increase in the thickness of laminar sub-layer which is characterized by poor heat transfer. Hence, the heat transfer co-efficient decreases beyond the relative pitch value of 10. Moreover, the number of turbulators also decreases with increasing pitch distance and hence the mixing effect brought about by the turbulators also decreases. This is verified from the turbulence intensity distribution plots as shown in Figure 10 which reveals the reduction in the number of higher turbulence intensity regions with increasing pitch distance. Therefore, the heat transfer enhancement brought about by the turbulators also decreases as indicated by a relatively lower levels of Nusselt number at larger relative pitch conditions as shown in Figure 6. Thus, the relative pitch of 10 is found to provide the highest increase in Nusselt number which is about 1.76 times higher in comparison to smooth duct at  $Re=9000$ .

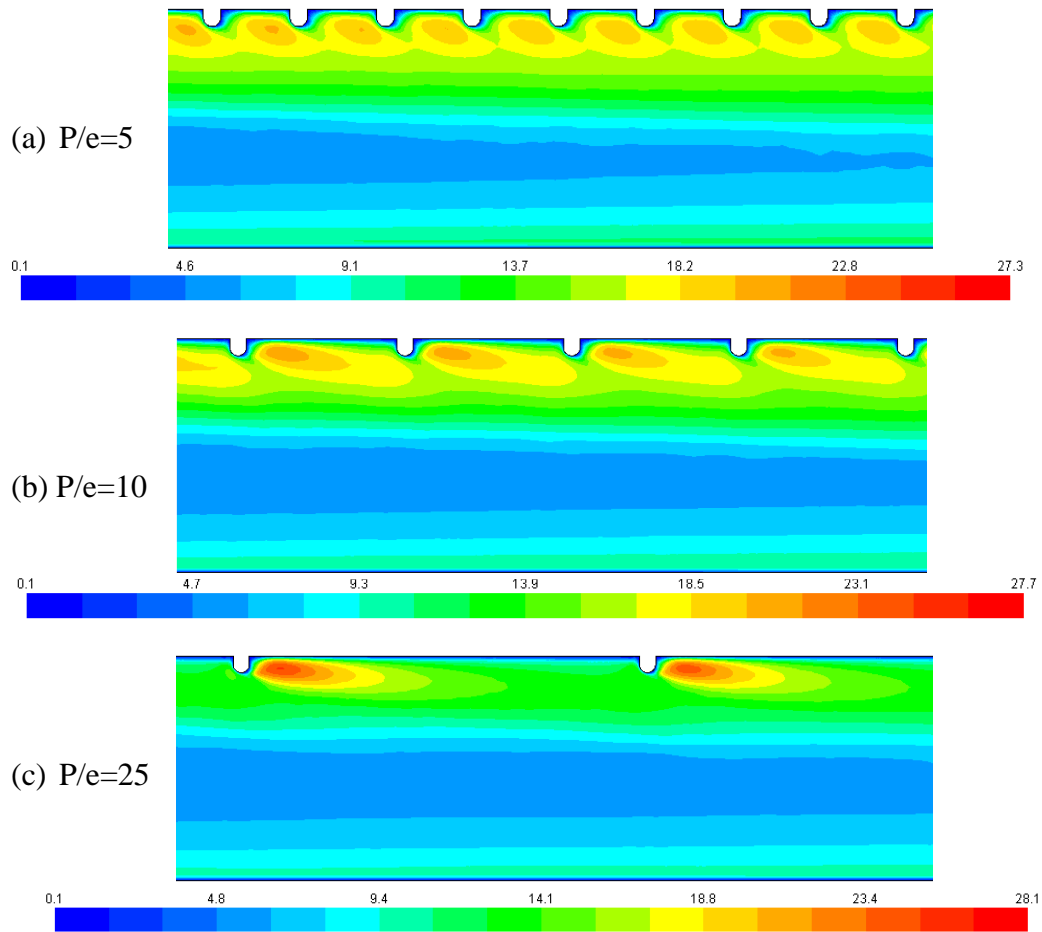


Figure10. Turbulence intensity distribution in the air flow across the rib for U-shaped rib turbulator for (a) P/e=5 (b) P/e=10 and (c) P/e=25 at Re=15,000.

### Friction Factor Characteristics

Figure 11 depicts the comparison of friction factor for the configuration of U-shaped turbulator for varying relative pitch values of 5, 10, 25 and 40 for the Reynolds number ranging between 9000 and 21,000. The friction factor results of U-shaped rib are compared with that of smooth duct which are determined using the well-known modified Blasius equation given by,

$$f_{smooth} = 0.085 Re^{-0.25} \quad (17)$$

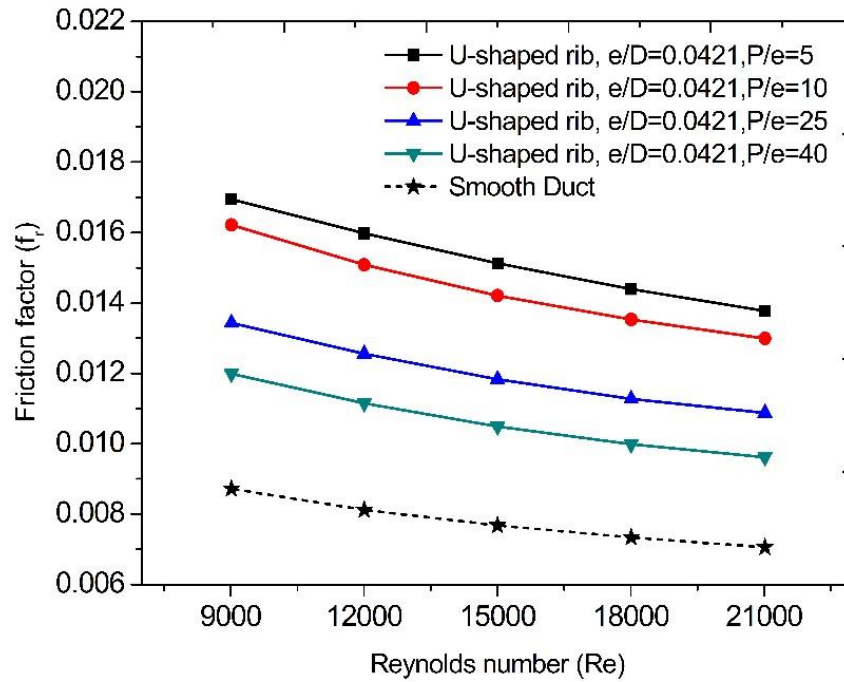


Figure 11. Comparison of friction factor for  $P/e=5, 10, 25$  and  $40$  at different flow Reynolds number.

From Figure 11, a general observation is that the use of U-shaped ribs increases the friction factor relative to the smooth duct at all flow rate conditions. This can be due to the presence of rib turbulators offer increased flow resistance viz., the pressure drag and viscous drag. Figure 12 shows the contour plot of static pressure around the rib region for varying relative pitch values at  $Re=15,000$ . It is seen that the static pressure rises on the upstream side of the rib due to flow impingement effect of the incoming flow. However, on the immediate downstream side of the rib, the static pressure drops due to the formation of low pressure recirculation zones. As a result, the presence of ribs introduce pressure drag in the air duct. In addition to this, the flow experiences viscous drag owing to viscous nature of the flow from the surfaces of reattachment region on the absorber plate as well as ribs excluding the surfaces covered by recirculation zones.

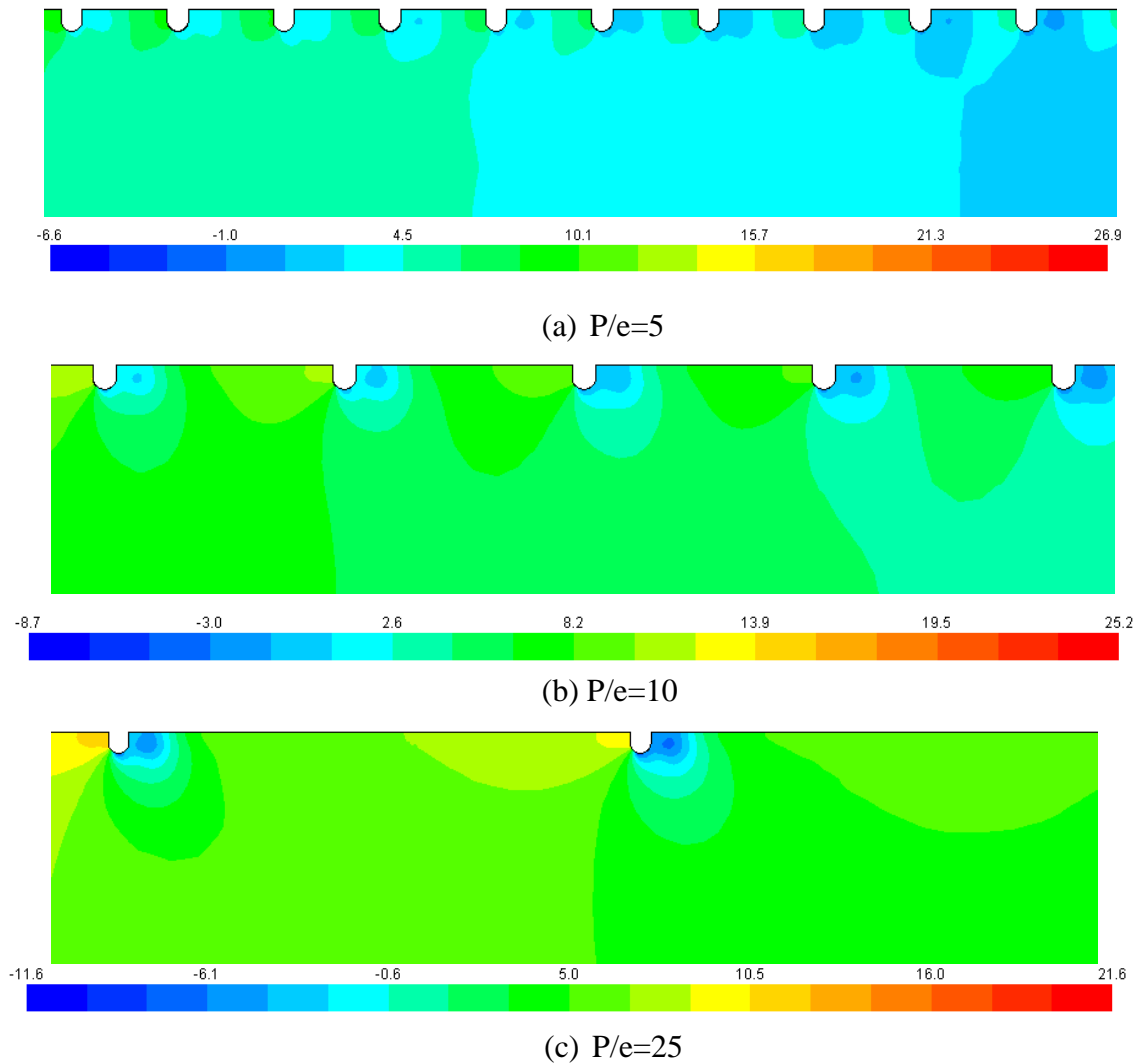


Figure 12. Static pressure distribution across the U-shaped rib turbulator for (a)  $P/e=5$  (b)  $P/e=10$  and (c)  $P/e=25$  at  $Re=15,000$ .

The combined effect of pressure and viscous drag leads to increased pressure energy loss and hence increased friction factor in the presence of ribs. The friction factor is also found to decrease with increasing values of relative pitch owing to lesser number of ribs on the absorber plate with increasing relative pitch values. This reduces the number of instances of flow disturbance caused by the ribs viz., flow acceleration, flow separation and flow reattachment. In particular, the flow acceleration reduces to a larger extent and the rise in static pressure due to flow impingement of accelerated flow decreases as shown in Figure 12. It is also observed that the rise in static pressure on the upstream side of each rib is relatively higher at lower values of relative pitch which ultimately results in the reduction of pressure drag. On the other hand, owing to increased distance between the reattachment point and the subsequent rib, the contact between the flow and the absorber surface increases thereby increasing the viscous drag. However, the rise in viscous drag is not significant enough as compared to the decrease in the pressure drag which results in an overall reduction in friction

factor. It is also noted that the friction factor decreases with increasing flow Reynolds number as shown in Figure 11. As the Reynolds number of the flow increases, the inertial forces become more dominant as compared to the viscous forces and the thickness of laminar sub-layer is reduced resulting in the reduction of viscous drag effect and hence the friction factor. Thus, it can be concluded that the friction factor increases with decreasing pitch values and the maximum friction factor enhancement is found to be about 1.95 for the relative height of 0.0421 and relative pitch of 5 at  $Re=21,000$ .

### Thermal Enhancement Factor

Thermal Enhancement Factor (TEF) takes into account the friction factor penalty imposed by the presence of ribs to achieve Nusselt number enhancement for a given flow Reynolds number and therefore indicates the effective thermal gain. The TEF value greater than 1.0 is desirable for a rib design to be acceptable as thermal enhancement device.

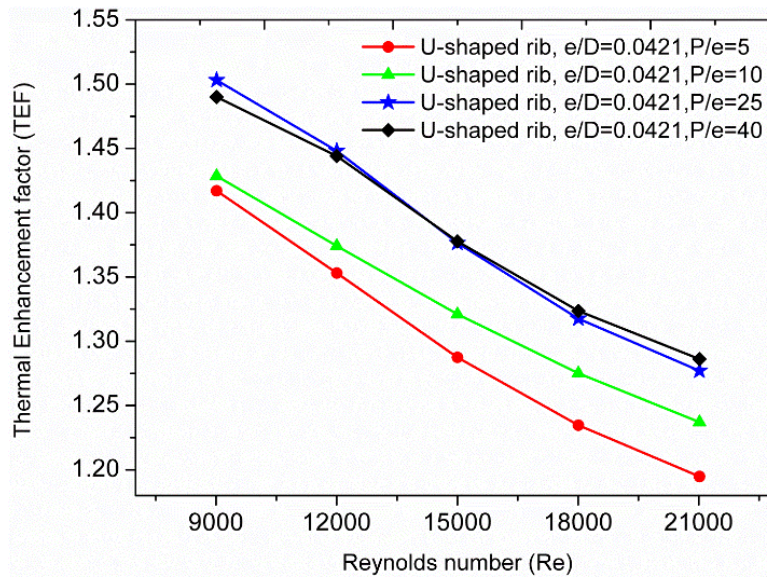


Figure 13. Variation of thermal enhancement factor for U-shaped turbulator for the configuration of  $e/D = 0.0421$  and  $P/e = 5, 10, 25$  and  $40$ .

Figure 13 depicts the variation of TEF for the configuration of U-shaped turbulator for varying relative pitch values of 5, 10, 25 and 40 for the Reynolds number ranging between 9000 and 21,000. It is observed that the configurations having higher pitch values provide higher TEF as compared to lower pitch configurations. This trend can be explained with reference to Figure 14 and Figure 15 which show the extents of Nusselt number enhancement and friction factor enhancement respectively. It is noted that despite having a relatively higher Nusselt number enhancement at lower pitch values as shown in Figure 14, the corresponding enhancement in friction factor is also higher as displayed in Figure 15 as a result of which higher pitch values exhibit relatively higher TEF. It is also noted that the TEF decreases with increasing flow Reynolds number. This is due to the fact that the Nusselt number enhancement is found to decrease with increasing flow rate as shown in Figure 14 while the friction factor enhancement does not vary considerably as shown in Figure 15.

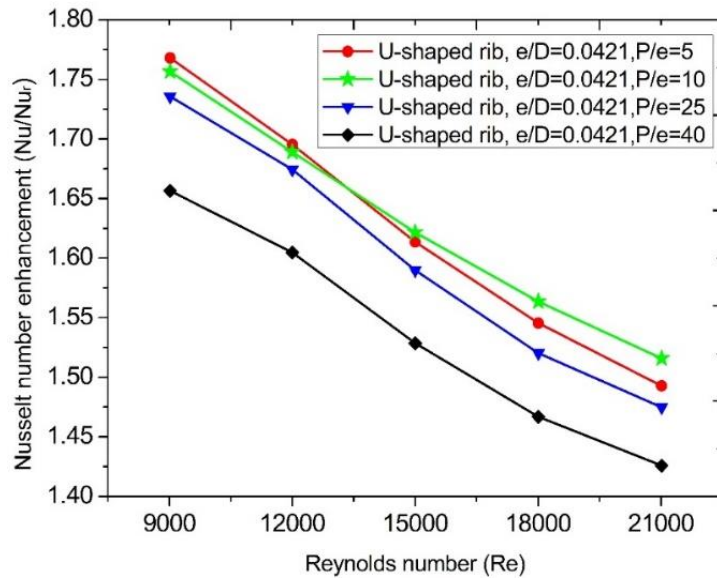


Figure 14. Nusselt number enhancement for U-shaped turbulator for the configuration of  $e/D = 0.0421$  and  $P/e = 5, 10, 25$  and  $40$ .

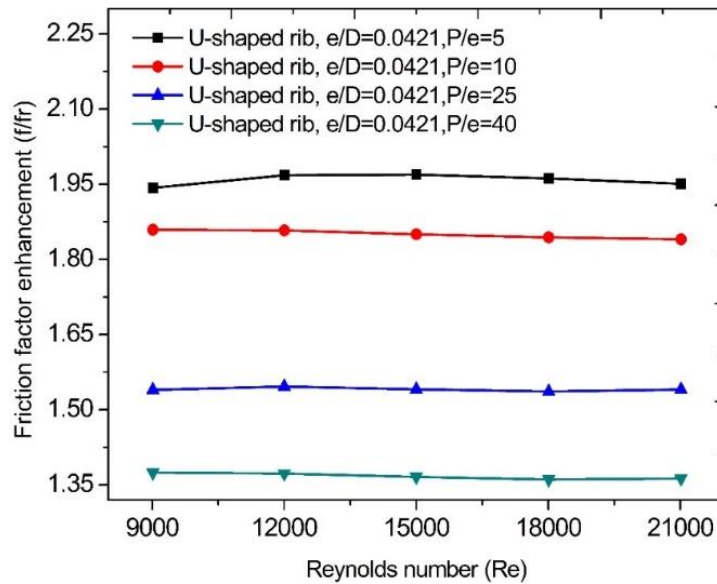


Figure 15. Friction factor enhancement for U-shaped turbulator for the configuration of  $e/D = 0.0421$  and  $P/e = 5, 10, 25$  and  $40$ .

The maximum TEF is found to be in the range of 1.5-1.28 for  $P/e=25$ . It is interesting to note that the rib configuration having  $P/e=40$  produces closer thermo-hydraulic performance as  $P/e=25$  for the range of flow Reynolds number considered in the analysis. From Figure 14, it is observed that the average Nusselt number enhancement is relatively higher at 1.6 for  $P/e=25$  as compared to that of 1.53 for  $P/e=40$ . However, the average enhancement in friction factor for  $P/e=25$  is relatively higher at 1.54 as compared to that of

1.37 for  $P/e=40$  as shown in Figure 15. Therefore, the effective thermal gain for both the pitches are comparable within the operating conditions used in the analysis. Thus, it can be deduced that it is beneficial to use relative pitch values ranging between 25 and 40 produce to achieve higher thermo-hydraulic performance.

### **COMPARISON OF U-SHAPED AND CIRCULAR RIB TURBULATOR**

The U-shaped rib can be perceived as a modified circular rib as per Figure 16 which shows that the straightening of curved edges of the upper half portion of circular rib leads to the formation of a U-shaped rib turbulator. The modification results in the elimination of corners in circular rib which could trap the air flow in the small region. Therefore, it is of interest to understand the changes brought about by this modification on the flow behavior and its corresponding impact on heat transfer.

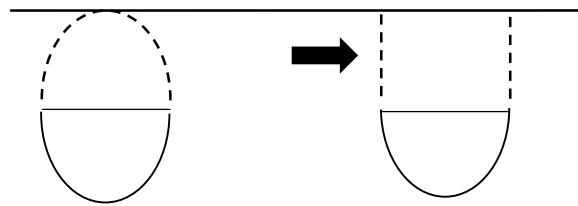


Figure 16. Transformation of circular rib geometry to U-shaped rib geometry through edge modification.

#### **Heat Transfer Characteristics**

Figure 17 depicts the comparison of Nusselt number for U-shaped rib and circular rib turbulators for the  $P/e=10$  and  $e/D=0.0421$  for the Reynolds number range of 9000-21,000. It is found that the U-shaped rib turbulator has higher Nusselt number relative to the circular rib at all flow rates used in the analysis. This can be explained with reference to Figure 18 which shows the pathline plots of velocity for both the U-shaped ribs and circular ribs. It is interesting to see that the flow structure of both the circular ribs and U-shaped ribs are similar except for the formation of an additional small sized low velocity recirculation zones on the upstream and downstream side of circular rib as highlighted in Figure 18. These slow moving recirculating zones remain entrapped in the small region between the absorber plate and curved edge of the circular rib and do not come in contact with the main flow for heat energy exchange thereby creating hot spots as shown by the temperature contour plots in Figure 19. These hot spots are the zones of low heat transfer which reduce the overall heat energy exchange from the absorber surface. On the other hand, the U-shaped ribs are characterized by the presence of hot spots only on the downstream side of the rib which are at a relatively lower temperature as compared to circular ribs. Therefore, the heat energy exchange from the U-shaped rib turbulator is relatively higher as compared to circular ribs as indicated by the relatively higher values of Nusselt number in Figure 17. The maximum Nusselt number for U-shaped rib turbulator is found to be about 15.65% higher as compared that of circular rib turbulator for  $Re=21,000$ .

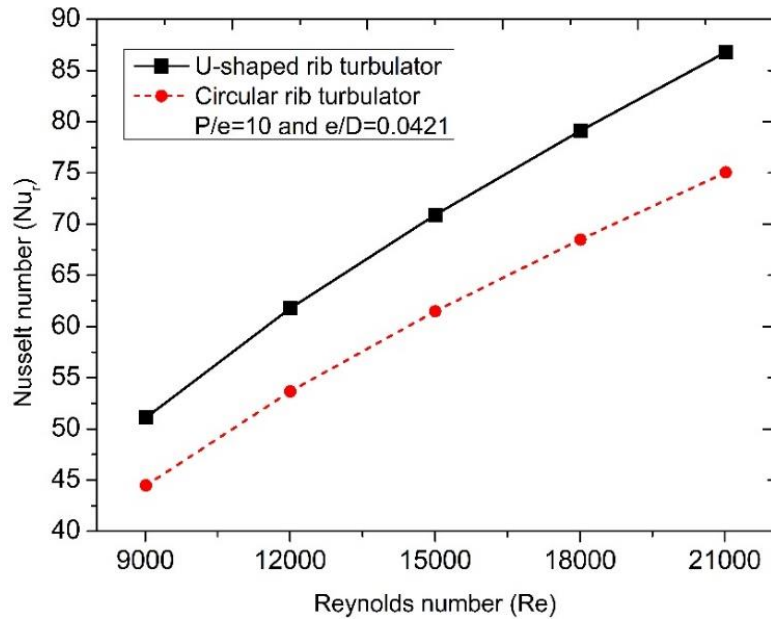


Figure 17. Comparison of Nusselt number for U-shaped rib and circular rib turbulators for  $P/e=10$  and  $e/D=0.0421$ .

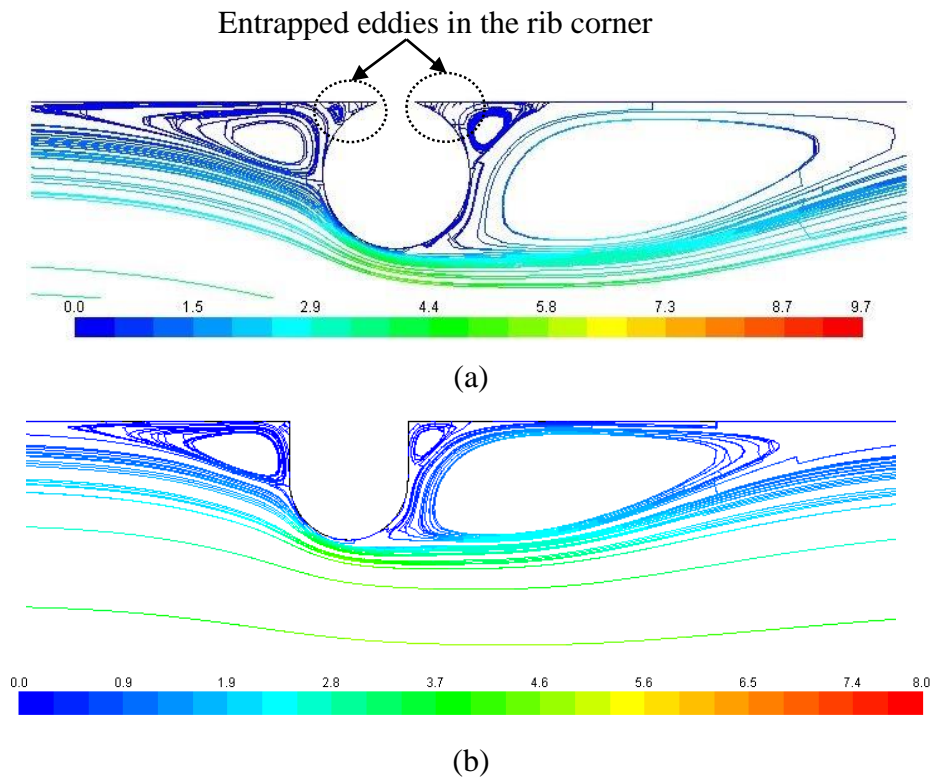


Figure 18. Comparison of pathline plots of air flow across U-shaped rib and circular rib turbulators for  $P/e=10$ ,  $e/D=0.0421$  and  $Re=15000$ .

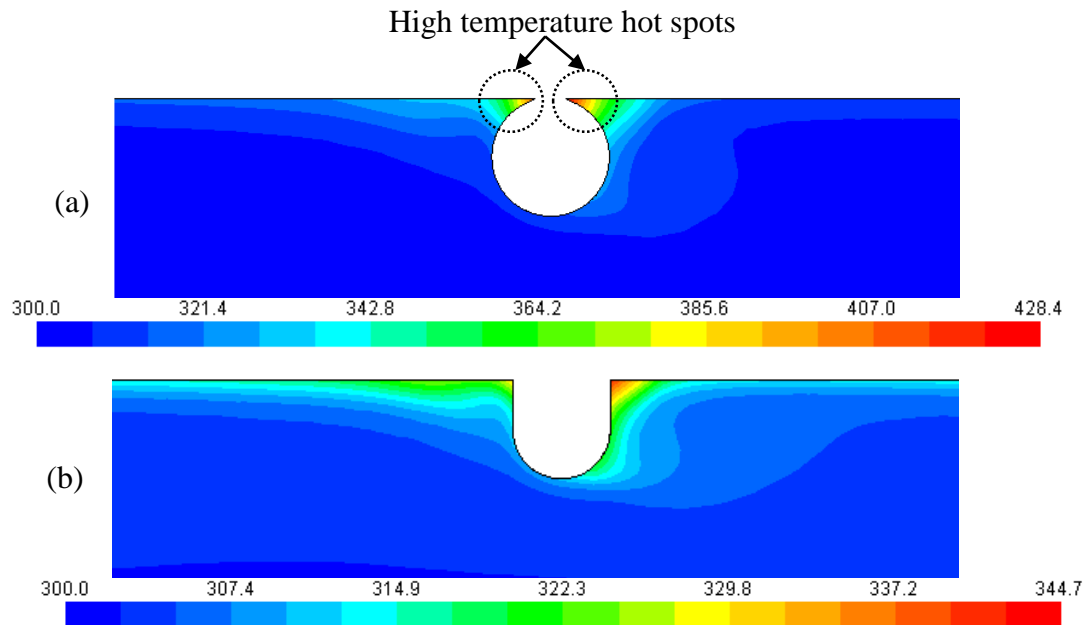


Figure 19. Comparison of temperature distribution in the air flow across (a) Circular rib and (b) U-shaped rib turbulator for  $P/e=10$ ,  $e/D=0.0421$  and  $Re=15000$ .

### Friction Factor Characteristics

Figure 20 shows the comparison of friction factor for U-shaped rib and circular rib turbulators for  $P/e=10$  and  $e/D=0.0421$  for the Reynolds number range of 9000-21,000. The friction factor for both the ribs is found to be nearly same at all flow rates owing to almost same static pressure changes across both rib shapes as revealed by the pressure contour plots in Figure 21 at  $Re=15000$ .

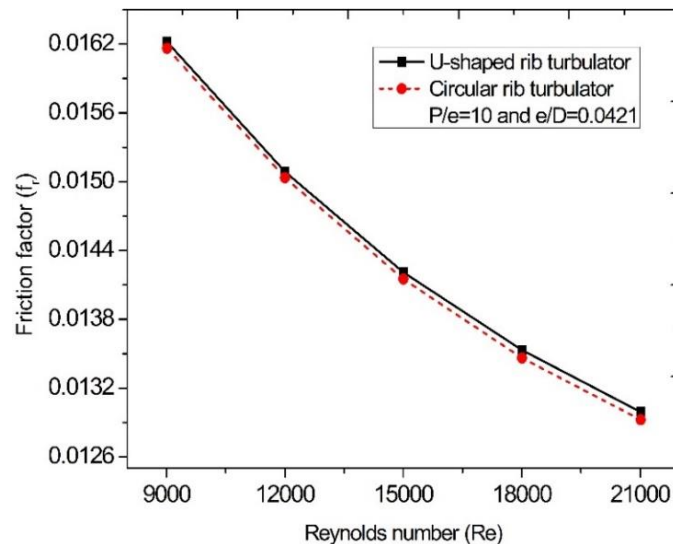


Figure 20. Comparison of friction factor for U-shaped and circular rib turbulators for  $P/e=10$  and  $e/D=0.0421$ .

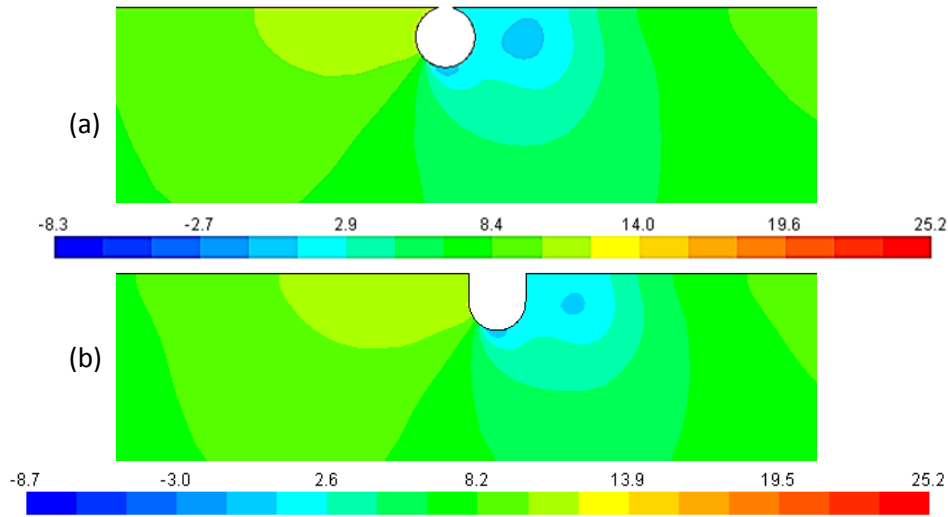


Figure 21. Comparison of pressure contour plots for U-shaped and circular rib turbulator for  $P/e=10$ ,  $e/D=0.0421$  and  $Re=15000$ .

**Thermal Enhancement Factor**

Figure 22 shows the comparison of Thermal Enhancement Factor (TEF) for  $P/e=10$  and  $e/D=0.0421$  for the Reynolds number range of 9000-21,000. It is found that the TEF for U-shaped rib is relatively higher for all the flow rates used in the analysis.

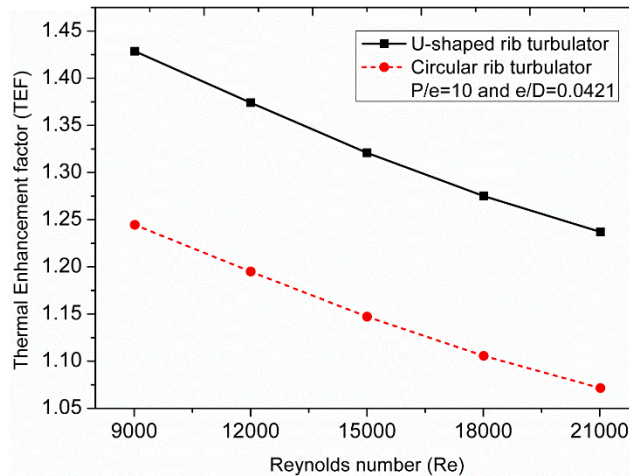


Figure 22. Comparison of Thermal Enhancement Factor (TEF) for U-shaped and circular rib turbulators for  $P/e=10$  and  $e/D=0.0421$ .

This is due a relatively higher Nusselt number enhancement for U-shaped rib while the friction factor enhancement remained nearly the same for both the ribs. Therefore, the effective thermal performance as indicated by the TEF is greater for U-shaped rib. The average increase in TEF for U-shaped rib is found to be about 15% higher as compared to the circular rib. Hence, it can deduced that the U-shaped rib turbulator is more effective in providing thermal performance enhancement relative to circular rib. Table 8 shows the

comparison of thermal performance factor of U-shaped rib with various rib geometries reported by previous researchers. It is seen that the U-shaped rib provides comparable enhancement in terms of thermal enhancement factor with respect to other reported rib geometries.

Table 8. Comparison of thermal enhancement factor (TEF) of U-shaped rib with other reported rib geometries

Rib geometry	Investigators	Maximum TEF	Corresponding optimum relative rib pitch
Square transverse ribs	Yadav and Bhagoria [2]	1.88	P/e=7.14
Square transverse ribs	Yadav and Bhagoria [3]	1.82	P/e=10.71
Square wave profiled rib	Singh and Singh [4]	1.43	P/e=10
Chamfered square ribs	Gawande et al.[5]	2.047	P/e=7.14
Transverse circular ribs	Yadav and Bhagoria [6]	1.65	P/e=10.71
Circular ribs with circular vortex generators in the duct entry section	Gawande et al. [7]	1.54	P/e=25
Semi-circular ribs	Yadav and Bhagoria [8]	1.71	P/e=14.29
Isosceles triangle rib	Ranjan et al. [9]	3.1	P/e=5
Right angled triangle rib	Gawande et al.[10]	2.03	P/e=7.14
Equilateral triangular Rib	Yadav and Bhagoria [11]	2.11	P/e=7.14
Transverse hyperbolic rib	Thakur et al. [13]	2.11	P/e=7.14
Reverse L-shaped ribs	Gawande et al.[14]	1.9	P/e=7.14
Tapered rectangular sectioned rib	Gupta and Varshney [15]	1.91	P/e=10.7
Rectangular rib with grooves	Jaurker et al. [19]	1.8	P/e=6
Square transverse ribs		1.62	
Trapezoidal rib with decreasing height in flow direction		1.6	
Trapezoidal rib with increasing height in flow direction	Kamali and Binesh [20]	1.54	P/e=12
Triangular rib		1.46	
Square rib		1.1	
30° chamfered square rib		1.11	
45° chamfered square rib		1.12	
60° chamfered square rib	Zheng et al. [21]	1.14	P/e=10
Concave rib		1.11	
Convex rib		1.13	
U-shaped rib	Present work	1.5	P/e=25

## CONCLUSIONS

A two dimensional CFD analysis using ANSYS Fluent software is conducted on a flat plate solar air heater to determine the efficacy of U-shaped rib turbulator for the flow Reynolds number range of 9000 to 21,000. The RNG k- $\epsilon$  turbulence model is used in the simulation study to capture the turbulence flow parameters. The results of Nusselt number, friction factor and Thermal enhancement factor for U-shaped rib turbulator are compared against that of the plain duct. The following conclusions can be drawn from the above analysis:

- Use of U-shaped rib results in increased friction factor with reference to smooth duct.
- The relative pitch of 10 is found to provide the highest increase in Nusselt number which is about 1.76 times higher in comparison to smooth duct at Re=9000.
- The friction factor increases with decreasing pitch values and the maximum friction factor enhancement is found to be about 1.95 for the relative height of 0.0421 and relative pitch of 5 at Re=21,000.
- The maximum TEF is found to be in the range of 1.5-1.28 for the configuration of P/e=25.
- It is beneficial to use relative pitch values ranging between 25 and 40 produce to achieve higher thermo-hydraulic performance.
- The U-shaped rib turbulator significantly reduces the hot spots at the rib corners in comparison to circular rib and is more effective in providing thermal performance enhancement as compared to circular rib.

## ACKNOWLEDGEMENTS

The authors thankfully acknowledge the computational facility extended by the School of Engineering and IT, MAHE Dubai Campus for carrying out the computer simulation study. The study did not receive any fund or grant from external agencies.

## REFERENCES

- [1] Al-Kayiem HH, Md Yunus Y. Drying of empty fruit bunches as wasted biomass by hybrid solar–thermal drying technique. *Journal of Mechanical Engineering and Sciences* 2013;5:652-661.
- [2] Anil SY, Bhagoria JL. A numerical investigation of square sectioned transverse rib roughened solar air heater. *International Journal of Thermal Sciences* 2014;79: 111–31.
- [3] Anil SY, Bhagoria JL. Numerical investigation of flow through an artificially roughened solar air heater, *International Journal of Ambient Energy* 2015;36:2, 87-100.
- [4] Inderjeet S, Sukhmeet S. CFD analysis of solar air heater duct having square wave profiled transverse ribs as roughness elements. *Solar Energy* 2018;162: 442–53.
- [5] Vipin G, Dhoble AS, Zodpe DB. Experimental and CFD-based thermal performance prediction of solar air heater provided with chamfered square rib as artificial

- roughness. *Journal of the Brazilian Society of Mechanical Sciences and Engineering* 2016;38(2):643.
- [6] Anil SY, Bhagoria JL. Heat transfer and fluid flow analysis of an artificially roughened solar air heater: A CFD based investigation. *Frontiers in Energy* 2014;8(2):201–11.
- [7] Vipin G, Dhoble AS, Zodpe DB. CFD analysis to study effect of circular vortex generator placed in inlet section to investigate heat transfer aspects of solar air heater. *The Scientific World Journal* 2014.
- [8] Anil SY, Bhagoria JL. A numerical investigation of turbulent flows through an artificially roughened solar air heater. *Numerical Heat Transfer; Part A: Applications* 2014;65(7):679–98.
- [9] Rajeev R, Paswan MK, Prasad N. CFD analysis of thermal performance in isosceles right triangle rib roughness on the absorber plate solar air heater. *Indian Journal of Science and Technology* 2016;9(38)
- [10] Vipin G, Dhoble AS, Zodpe DB, Sunil Chamoli. Experimental and CFD-based thermal performance prediction of solar air heater provided with right-angle triangular rib as artificial roughness. *Journal of the Brazilian Society of Mechanical Sciences and Engineering* 2016;38(2):551-579.
- [11] Anil SY, Bhagoria JL. A CFD based thermo-hydraulic performance analysis of an artificially roughened solar air heater having equilateral triangular sectioned rib roughness on the absorber plate. *International Journal of Heat and Mass Transfer* 2014;70:1016–39.
- [12] Bhagoria J, Saini J, Solanki S. Heat transfer coefficient and friction factor correlations for rectangular solar air heater duct having transverse wedge shaped rib roughness on the absorber plate. *Renewable Energy* 2002;25(3):341–369.
- [13] Deep ST, Mohammed Kaleem Khan, Manabendra Pathak. Performance evaluation of solar air heater with novel hyperbolic rib geometry. *Renewable Energy* 2017;105:786–97.
- [14] Vipin G, Dhoble AS, Zodpe DB, Sunil Chamoli. Experimental and CFD investigation of convection heat transfer in solar air heater with reverse L-shaped ribs. *Solar Energy* 2016;131:275–95.
- [15] Gupta AD. and Varshney L. Performance prediction for solar air heater having rectangular sectioned tapered rib roughness using CFD. *Thermal Science and Engineering Progress* 2017;4:122–132.
- [16] Kumar R, Goel V, Kumar A. Investigation of heat transfer augmentation and friction factor in triangular duct solar air heater due to forward facing chamfered rectangular ribs: A CFD based analysis. *Renewable Energy* 2018;115:824–835.
- [17] Menni Y., Azzi A, Chamkha AJ. Optimal thermo aerodynamic performance of S-shaped baffled channels. *Journal of Mechanical Engineering and Sciences* 2018;12(3):3888 - 3913.
- [18] Gilani SE, Al-Kayiem HH, Woldemicheal DE. Effect of conical pin arrangement on heat transfer efficiency of a free convective solar air heater. *Journal of Mechanical Engineering and Sciences*. 2016;10:2:2053-2064.
- [19] Jaurker AR, Saini JS, Gandhi BK. Heat transfer and friction characteristics of rectangular solar air heater duct using rib-grooved artificial roughness. *Solar Energy* 2006;80(9):895–907.

- [20] Kamali R, Binesh AR. The importance of rib shape effects on the local heat transfer and flow friction characteristics of square ducts with ribbed internal surfaces. *International Communications in Heat and Mass Transfer* 2008;35:1032-1040.
- [21] Shaofei Z, Tingwu Ji, Gongnan Xie, Bengt Sunden. On the improvement of the poor heat transfer lee-side regions of square cross-section ribbed channels. *Numerical Heat Transfer Part A: Applications: An International Journal of Computation and Methodology* 2014;66(9):963-989.
- [22] Gupta D, Solanki SC, Saini JS. Heat and fluid flow in rectangular solar air heater ducts having transverse rib roughness on absorber plates. *Solar Energy* 1993;51(1):31-37.
- [23] ANSYS FLUENT documentation, ANSYS Inc.